Pol. J. Environ. Stud. Vol. XX, No. X (XXXX), 1-17
DOI: *10.15244/pjoes/204187* ONLINE PUBLICATION DATE:

Original Research

Water Quality Inversion for Tidal Surge on Qiantang River Based on UAV Multispectral Remote Sensing and Machine Learning

Ruohua Li[1], Sidan Lin[2], Mengya Zhao[2], Bingwei Zhang[3], Jixiong Chen[2], Lifang Hu[2], Tao Ding[2]*

[1]Zhejiang Tongji Vocational College of Science and Technology, Hangzhou, 311231, China
[2]Department of Environmental Engineering, China Jiliang University, Hangzhou, Zhejiang, 310018, China
[3]Zhejiang Institute of Hydraulics & Estuary, Hangzhou, Zhejiang, 310020, China

Received: 23 January 2025
Accepted: 19 April 2025

Abstract

By leveraging drone remote sensing technology, this study addresses the limitations of traditional monitoring methods in expansive water bodies, such as restricted sampling points, data acquisition challenges, and insufficient spatiotemporal resolution. It overcomes challenges, including synchronous data acquisition in dynamic tidal bore environments and nonlinear relationship modeling. Focusing on Qibao and Yanguan stations along the Qiantang River, the research integrates in-situ water quality data and multispectral remote sensing images during tidal bores. Machine learning models—Support Vector Machine Regression (SVR), Random Forest (RF), and eXtreme Gradient Boosting (XGBoost)—were developed to invert suspended sediment concentration (SSC) and turbidity. Bayesian Optimization was applied to enhance model performance. Results demonstrate that the XGBoost model optimized by the Bayesian algorithm achieved superior accuracy, with determination coefficients (R^2) of 0.89 (SSC) and 0.93 (turbidity), and reduced root mean square errors to 310.54 mg/L and 33.36 NTU, confirming model stability and predictive capability. Inversion results revealed abrupt SSC and turbidity surges near bridge piers during flood tides (peaking at 6000 mg/L and 820 NTU), indicating intense bed scouring by tidal bore dynamics. The model effectively captures spatiotemporal patterns of water quality parameters and provides an efficient solution for dynamic tidal bore monitoring, highlighting the potential of integrating multispectral imagery with machine learning. This approach offers a novel framework for high-frequency water quality assessment in turbulent hydrodynamic environments.

Keywords: multispectral, machine learning, remote sensing inversion, suspended solids concentration, turbidity

*e-mail: dingtao@cjlu.edu.cn
Tel.: +86-571-13757133532

Introduction

The Qiantang River, which is the largest water system in Zhejiang Province, China, is known as the world-famous Qianjiang Tidal Bore [1]. This magnificent natural spectacle is caused by the rapid narrowing of the river surface and the rapid uplift of the riverbed after tidal waves from the East China Sea surge into Hangzhou Bay. While the tidal bore gives the Qiantang River its unique natural landscape, it also has a direct and significant impact on water quality [2, 3]. The periodic changes in water flow caused by the tidal bore bring a large amount of seawater, sediment, and other materials, severely affecting the spatial and temporal distribution patterns of various water quality parameters such as salinity [4, 5], suspended solids concentration [6, 7], and turbidity [8] in the Qiantang River. This, in turn, leads to issues such as sediment deposition and water pollution, which adversely affect the sustainable economic and social development of coastal areas, the health of ecosystems, drinking water safety for residents, and agricultural irrigation [9-12]. Therefore, it is crucial to monitor the water quality of the Qiantang River during the tidal bore.

Currently, water quality monitoring of the Qiantang River tidal bore mainly relies on two methods: on-site manual sampling and laboratory analysis and water quality automatic monitoring stations [13, 14]. On-site manual sampling involves collecting water samples in the field and analyzing them in a laboratory to monitor water quality. Although this method can provide detailed and accurate water quality data, the monitoring and analysis process is complex, time-consuming, and expensive, and the results only reflect the water quality at specific sampling points [15]. Especially during tidal periods, traditional manual sampling methods face significant challenges, and accurate measurements are almost impossible. On the other hand, water quality automatic monitoring stations rely on fixed observation stations to monitor the water quality of the Qiantang River in real-time throughout the day. However, in actual operation, there are issues such as high maintenance costs, susceptibility of monitoring instruments to strong tides, damage, and limited monitoring station locations [16]. Therefore, it is necessary to find more effective monitoring methods to meet the water quality monitoring requirements during the Qiantang River tidal bore.

Due to its capability for straightforward dynamic monitoring, researchers have increasingly adopted remote sensing technology to address real-world challenges. For instance, Morakot et al. [17] utilized satellite imagery combined with supervised classification and change detection techniques to quantify the persistent agricultural land loss over two decades in a Thai province, providing a scientific basis for regional sustainable development. Compared to various remote sensing technologies, drone-based remote sensing has emerged as a promising tool for water quality monitoring due to its advantages in low cost, portability, flexible deployment, and operational independence from fixed locations or strict scheduling [18-20]. This method not only reduces the risks associated with sampling but also enhances monitoring safety and environmental friendliness. It enables quick response and real-time monitoring of the dynamic changes in the Qiantang River tidal bore water quality, providing rich and comprehensive information on water quality conditions and spatial distribution [21-23]. Traditional remote sensing inversion methodologies predominantly encompass analytical approaches [24], empirical techniques [25], and semi-empirical methods [26]. The evolution of artificial intelligence technology has led to a growing number of studies integrating machine learning principles into water quality remote sensing monitoring [27-29]. Machine learning boasts attributes such as adaptability, self-learning capabilities, high efficiency, and fault tolerance, positioning it as a potent strategy for addressing intricate issues characterized by multiple variables and non-linearity. It holds certain advantages in estimating water quality [30-32]. For instance, Rabsh et al. [33] developed an index prediction model using Artificial Neural Networks (ANN) and conducted a comparative analysis of three models – Recurrent Fuzzy Networks (RFN), Backpropagation Networks (BPN), and Feedforward Neural Networks (FNN)—ultimately identifying the FNN model as the most effective for water quality prediction in the Klang River, offering a scalable, intelligent tool for river management. The predictive capabilities of machine learning further extend to forecasting future scenarios of water quality parameters. For example, Jantira et al. [34] integrated satellite imagery with a CA-Markov model to analyze 30-year land use and land cover dynamics in the Bandung Bay region and projected trends for the subsequent three decades. These cases collectively demonstrate the feasibility of combining remote sensing technology with algorithmic models for robust water quality estimation.

In water quality studies, the integrated impact of multiple parameters on aquatic ecosystem functions warrants critical attention. There has been growing interest in water quality classification research based on statistical models and comprehensive evaluation methods in recent years. For instance, Kieu et al. [35] evaluated surface water quality in Can Tho City, Vietnam, by analyzing 18 parameters across 38 monitoring sites during the dry and rainy seasons using the Eutrophication Index (EI), Harmony Degree Equation (HDE), and entropy-weighted TOPSIS method. Their findings revealed persistent exceedances of total suspended solids (TSS) and fecal coliform levels in both seasons. While such methods offer novel insights into multi-parameter synergistic assessment and priority management, their applicability to highly dynamic tidal bore environments with pronounced spatiotemporal variability remains underexplored.

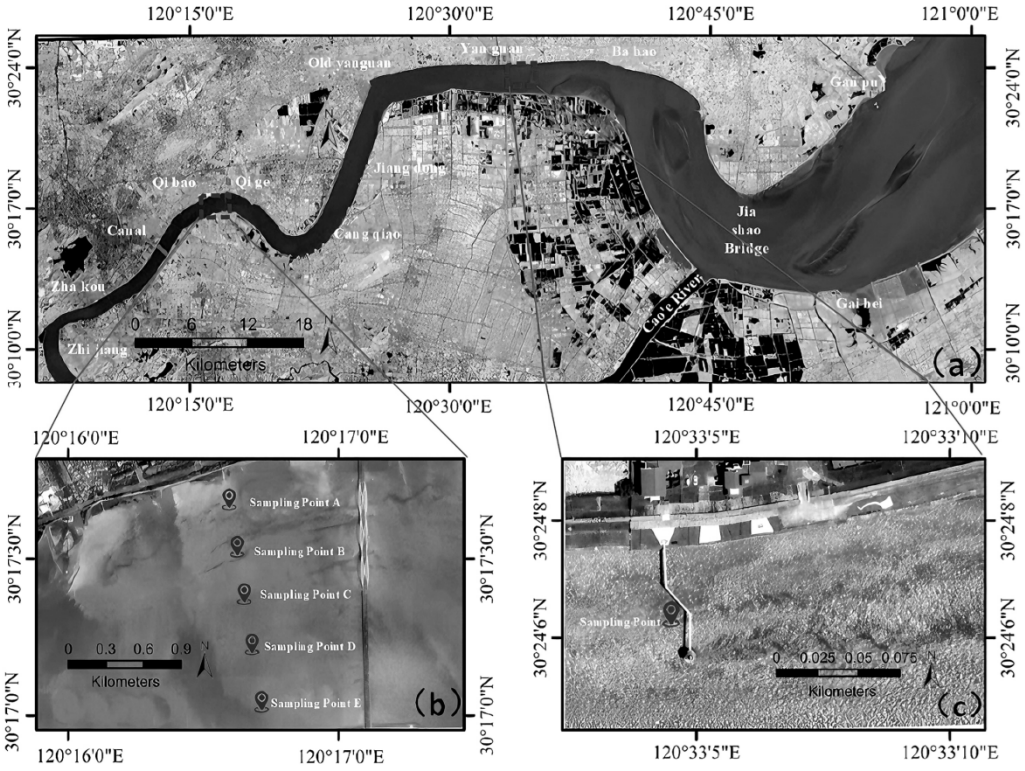

Fig. 1. Study area: (a) the entire Qiantang River basin; (b) distribution of sampling points at Qibao station; (c) distribution of sampling points at Yanguan station.

This study addresses three core challenges in tidal bore monitoring. (1) Synchronization of dynamic data acquisition: The ephemeral nature of tidal bores necessitates precise spatiotemporal alignment between rapid image capture and high-frequency water sampling. (2) Mitigation of spectral interference: Intense tidal currents induce ripple-induced distortions and uneven suspended sediment distribution, amplifying noise in multispectral reflectance data. (3) Enhanced model generalizability: Conventional machine learning models, though effective in static water bodies, struggle with the complex nonlinear relationships between spectral features and water quality parameters under turbulent tidal bore conditions, often leading to overfitting.

To overcome these challenges, three targeted strategies were implemented. (1) Dynamic coordinated sampling system: Integrating real-time kinematic (RTK) positioning with tidal forecasting minimizes temporal mismatches. (2) Noise-adaptive spectral correction: Statistical averaging mitigated local fluctuations, while radiometric compensation addressed illumination variability. (3) Dual-layer feature optimization: A hybrid approach combining Pearson correlation coefficient analysis and random forest-based recursive feature elimination (RF-RFE) was employed to select optimal spectral predictors. This informed the development of a Bayesian-optimized XGBoost hybrid model (BO-XGBoost), which efficiently identifies global hyperparameter optima within limited iterations, significantly enhancing model stability in transient hydrodynamic environments.

Based on the aforementioned context, this study selects the Qiantang River's Qibao Station and Yanguan Station as the research areas. Integrating the actual water quality data gathered during two tidal bore events on November 16th and 28th, 2023, with the synchronized multispectral remote sensing image data, a machine learning-based inversion model for suspended solids concentration and turbidity is constructed. The laws of spatiotemporal variation and influencing mechanisms are analyzed. The research findings validate the feasibility of multispectral imagery and machine learning inversion models in tidal bore water quality monitoring, providing a new thought process and method for tidal bore water quality monitoring endeavors.

Materials and Methods

Study Area

The research was conducted within the Qiantang River basin, situated in Zhejiang Province, China. The basin encompasses an area from 117°37' to 121°52' E longitude and from 28°10' to 30°48' N latitude, characterized by a subtropical monsoon climate with an average annual temperature of 17°C. The tidal reach of the Qiantang River, extending 291 km from the Fuchun River Power Station to Hangzhou Bay, is

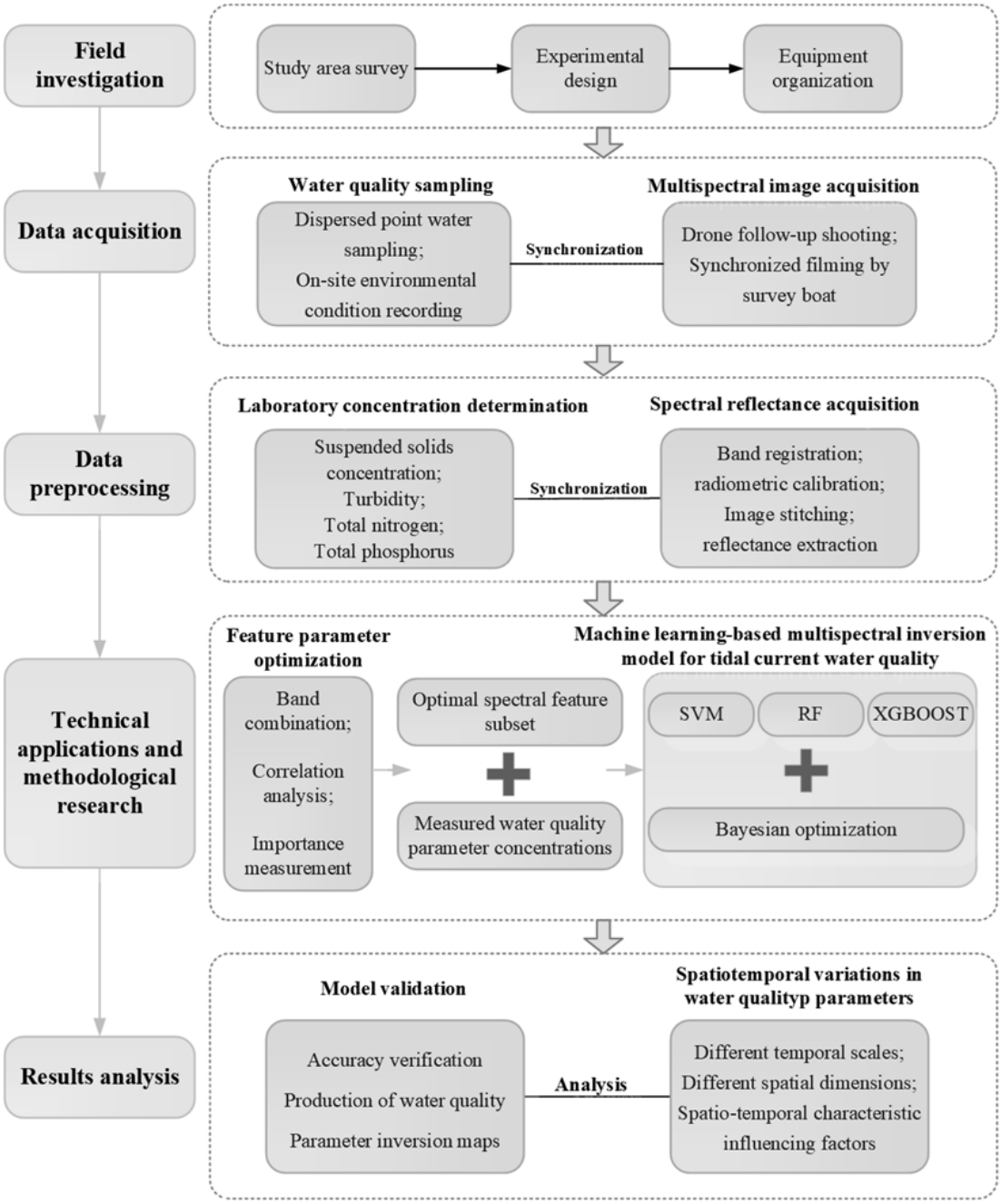

Fig. 2. Technical roadmap.

designated as the Qiantang River Estuary. This estuary is a prototypical strong tidal estuary, subjected to the interplay of river runoff and tidal currents. The water quality parameters in this region demonstrate significant spatiotemporal variations closely linked to the rise and fall of tidal bores. Therefore, this study selected two representative sites within the estuarine zone, Qibao and Yanguan, as the research areas (Fig. 1). Both sites are affected by tidal bores, with Yanguan positioned downstream experiencing more pronounced impacts from tidal bores.

Technical Roadmap

To achieve effective remote sensing monitoring of tidal water quality in the Qiantang River, the entire process can be summarized into five stages (Fig. 2): field investigation, data acquisition, data preprocessing, technical applications and methodological research, and results analysis.

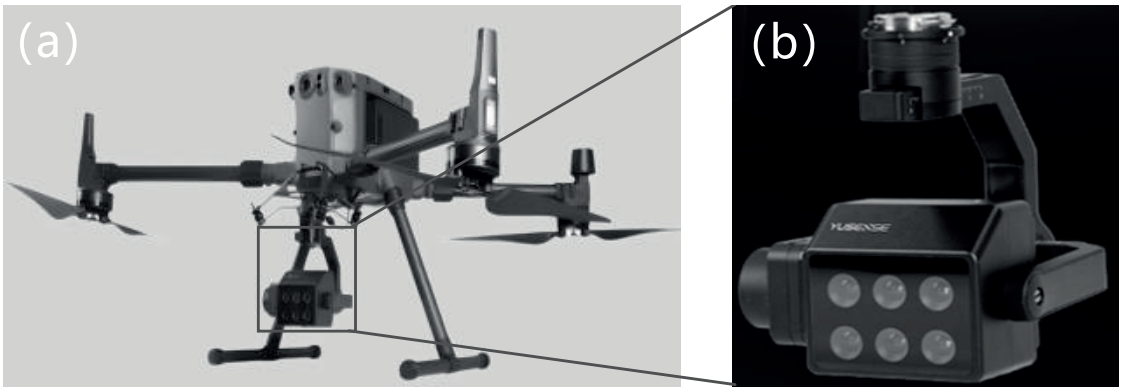

Fig. 3. Image acquisition platform: (a) DJI M300RTK Unmanned Aerial Vehicle; (b) MS600 Pro multispectral camera.

Data Acquisition and Preprocessing

Sub-subsection

The initial water sampling was executed at the Qiantang River Qibao Station on November 16, 2023, between 8:00 and 17:00 (lunar calendar, the 4th day of the 10th month, coinciding with the spring tide period). A total of ten rounds of sampling were conducted hourly from sampling points A to E, encompassing both the flood and ebb tide processes. However, the surge intensity was notably diminished on the actual sampling date due to unexpectedly strong winds. To maintain the integrity of the data, additional sampling was performed at Yanguan Station, which experienced a more pronounced surge on November 28, from 11:30 to 14:00 (lunar calendar, the 16th day of the 10th month, during the spring tide). The sampling at Yanguan Station primarily focused on the period immediately before and after the flood tide. Data collection was conducted every 20 minutes before the surge's arrival to precisely capture the data fluctuations during the flood tide, totaling three instances. It was observed on-site that the surge arrived after the third sampling, at which time the sampling frequency was increased to every 5 minutes and sustained for a continuous span of 20 samplings.

During the collection of water samples, sampling point locations were accessed by a survey boat. Once the water flow stabilized, a professional water pump extracted 1000mL of water at a depth of 0.5 meters below the surface. These water samples were then transferred into pre-prepared, dry, and clean water sample bottles, labeled, and reserved for subsequent analysis of suspended solids concentration and turbidity. The on-site parameters of this sampling site were simultaneously recorded. These on-site parameters include sampling time, sample number, latitude and longitude coordinates, light intensity, and other factors. The water samples were promptly transported to the laboratory for concentration measurements following standardized testing procedures. The measurement of suspended solids concentration adhered strictly to the national standard GB17378.4-2007, utilizing the gravimetric method. The turbidity of the samples was assessed using a HACH2100Q portable turbidity meter, with three replicate measurements conducted for each sample, and the average value was calculated.

Acquisition and Preprocessing of Multispectral Imagery

The acquisition of Unmanned Aerial Vehicle (UAV) multispectral imagery and water quality sampling is conducted simultaneously. The DJI M300 RTK UAV (DJI Innovations Technology Company, Shenzhen, Guangdong, China) was equipped with the MS600 Pro multispectral camera (Changguang Yuchen Information Technology and Equipment Co., Ltd., Qingdao, Shandong, China) as an image acquisition platform (Fig. 3). Fixed-point aerial photography was separately conducted at sampling points of the Qibao Station and Yanguan Station. The flight altitude was set at 80m, with a ground spatial resolution of 5.77cm/pixel and an imaging swath of 74m×55m. A total of 538 sets of multispectral images with RTK positioning were obtained.

Following data acquisition, preprocessing was performed on the raw multispectral imagery, encompassing band registration, image stitching, radiometric correction, and other procedures. This procedure culminated in a TIFF image comprising six bands. Subsequently, the six-band TIFF image was imported into the remote sensing image processing platform ENVI 5.3. Pixel values were extracted by leveraging the latitude and longitude information, and a 9x9 pixel-sized region of interest (ROI) was delineated near the sampling point within the spectral image. The average spectral reflectance of each band within this ROI was computed and documented as the reflectance data for the respective sampling point.

Optimization and Selection of Spectral Feature Parameters

Two feature selection methods, namely the Pearson correlation coefficient [36] and recursive feature elimination based on Random Forest [37], were

employed to optimize and select the spectral feature parameters. Initially, the reflectance values of the six bands in the multispectral imagery were denoted as R1, R2, R3, R4, R5, and R6. Drawing from existing research, it has been found that commonly used band calculation methods include the Difference Index (DI), Ratio Index (RI), and Normalized Difference Index (NDI). These band calculation methods were introduced to construct three forms of spectral feature parameters [38].

The Pearson correlation coefficient was utilized to assess the degree of correlation between water quality parameters and various spectral feature parameters. This coefficient ranges from -1 to 1, with higher absolute values indicating a stronger correlation. The formula for calculating the Pearson correlation coefficient is as follows:

$$r = \frac{\sum (x_i - \bar{x})(y_i - \bar{y})}{\sqrt{\sum (x_i - \bar{x})^2 (y_i - \bar{y})^2}} \quad (1)$$

where: r represents the Pearson correlation coefficient; x_i represents the spectral feature parameter values of the sampling points; y_i represents the concentration values of water quality parameters at the sampling points; $\bar{x}$ represents the average value of spectral feature parameters at the sampling points; $\bar{y}$ represents the average value of water quality concentration parameters.

Due to the potential existence of complex nonlinear relationships between spectral feature parameters and water quality parameters, relying solely on the Pearson correlation coefficient may not suffice to fully uncover their underlying correlations. The additional step of re-optimizing the spectral feature parameters has been introduced by employing the Recursive Feature Elimination based on Random Forest (RF-RFE). The specific steps are as follows: Initially, the out-of-bag data prediction accuracy of the Random Forest is utilized to calculate the importance of each spectral feature parameter; subsequently, the currently least important feature is removed; the model is constantly retrained, and the training process is repeated iteratively until the predetermined number of features is reached; when the stopping condition is met, the final feature subset emerges as the optimal feature subset for water quality parameter inversion. This feature subset is employed as input to the tidal bore water quality inversion model to enhance its generalization performance.

Construction and Evaluation of the Inversion Model

The optimal feature subset is utilized as the independent variable, and the measured values of water quality parameters serve as the dependent variable to construct tidal water quality inversion models based on Support Vector Machine Regression (SVR) [39], Random Forest (RF) [40], and Extreme Gradient Boosting (XGBoost) [41]. Concurrently, the Bayesian Optimization algorithm (BO) [42] is applied to optimize the hyperparameters of these three machine learning models, resulting in the Bayesian Optimization-based Support Vector Machine Regression (BO-SVR), Bayesian Optimization-based Random Forest (BO-RF), and Bayesian Optimization-based Extreme Gradient Boosting (BO-XGBoost) inversion models. Bayesian Optimization is a heuristic global optimization method grounded in the probability distribution, capable of intelligently searching for the global optimal parameter combination within a limited number of iterations [43]. The specific optimization steps are as follows: Several sets of hyperparameters are randomly generated as initial points to establish the initial regression models; a Gaussian process model is constructed based on these initial points and their corresponding objective function values to model and predict the parameter space; the acquisition function PI is used to seek the next hyperparameter combination that is most likely to enhance model performance; determine if the set maximum iteration count has been reached; if not, iteration continues; otherwise, the optimal hyperparameter combination and the corresponding optimal value of the objective function for the regression model are output [44].

To quantitatively compare the inversion performance of the models, this study employs three evaluation metrics to assess the accuracy of water quality inversion models. These evaluation metrics include the coefficient of determination (R^2), root mean square error (*RMSE*), and mean absolute error (*MAE*). The formulas for these metrics are as follows:

$$R^2 = 1 - \frac{\sum_{i=1}^{n}(y_i - \hat{y}_i)^2}{\sum_{i=1}^{n}(y_i - \bar{y}_i)^2} \quad (2)$$

$$RMSE = \sqrt{\frac{1}{n}\sum_{i=1}^{n}(y_i - \hat{y}_i)^2} \quad (3)$$

$$MAE = \frac{1}{n}\sum_{i=1}^{n}[y_i - \hat{y}_i] \quad (4)$$

where: y_i and $\widehat{y_i}$ represent the predicted values and actual measured values of the model, respectively; $\bar{y_i}$ represents the mean of the actual measured values; n represents the number of water quality samples. The closer R^2 is to 1, and the smaller the *RMSE* and *MAE* are, the higher the model's accuracy is.

Table 1. Spectral Feature Parameters.

Combination Methods	Spectral Feature Parameters	
Single Band	R_i	i=1-6
Differential Index (DI)	R_i-R_j	i,j=1-6 and $j \neq i$
Ratio Index (RI)	R_i/R_j	i,j=1-6 and $j \neq i$
Normalized Index(NDI)	$(R_i-R_j)/(Ri+Rj)$	i,j=1-6 and $j \neq i$

Results and Discussion

Optimization and Selection of Spectral Feature Parameters

A total of 51 spectral feature parameters were determined by analyzing both individual bands and computed band combinations (Table 1). Pearson correlation analysis was conducted separately between these 51 spectral feature parameters and the measured values of suspended solids concentration and turbidity at field sampling points. It was observed that the correlation between suspended solids concentration, turbidity, and individual band spectral feature parameters was generally low. However, a higher correlation was observed between these water quality and spectral feature parameters constructed using ratio and normalization indices. Based on the correlation analysis, spectral feature parameters were selected if they achieved statistical significance ($p < 0.05$) and had a correlation coefficient absolute value (r) exceeding 0.6. These selected spectral feature parameters were considered subsets of features for each water quality parameter. Consequently, 32 sets of spectral feature parameters were identified that met the requirements for the inversion of suspended solids concentration and turbidity (Table 2).

Among all spectral feature parameters, the normalized difference index (R4-R5)/(R4+R5) exhibited the most significant correlations with suspended sediment concentration (SSC) and turbidity. Specifically, their absolute Pearson correlation coefficients reached 0.866 for SSC and 0.943 for turbidity, both indicating strong predictive relationships.

Recursive feature elimination with random forest (RF-RFE) was applied to further refine feature selection, identifying 10 optimal spectral indices for each target parameter. For SSC, the optimal feature subset comprised: {'R2-R3', 'R3-R4', 'R3-R5', 'R1/R5', 'R3/R4', 'R4/R5', '(R1-R3)/(R1+R3)', '(R3-R4)/(R3+R4)', '(R3-R5)/(R3+R5)', '(R4-R5)/(R4+R5)'}. For turbidity, the selected subset included: {'R1-R5', 'R2-R5', 'R3-R4', 'R1/R5', 'R2/R4', 'R2/R5', '(R1-R5)/(R1+R5)', '(R2-R5)/(R2+R5)', '(R3-R4)/(R3+R4)', '(R3-R5)/(R3+R5)'}.

Accuracy Evaluation of Water Quality Inversion Model

Accuracy Verification of Suspended Solids Concentration Inversion Model

Six suspended solids concentration inversion models, which were based on SVR, RF, XGBoost, BO-SVR, BO-RF, and BO-XGBoost, respectively, underwent accuracy verification (Table 3).

A comprehensive comparison of six models for suspended solids concentration inversion reveals that the inversion model based on BO-XGBoost outperforms others in all evaluation indicators. The model exhibits an exceptionally high R^2 value of 0.93, and it achieves the lowest values for both *RMSE* and *MAE;* therefore, it is the most outstanding model of all models. Additionally, the R^2 values of the SVR, RF, and XGBoost inversion models were respectively enhanced by 13.0%, 4.9%, and 4.7% after applying Bayesian Optimization techniques. This demonstrates the effectiveness of Bayesian Optimization in enhancing the accuracy of inversion models. In conclusion, the model based on BO-XGBoost exhibits the highest accuracy and the smallest errors in the inversion of tidal suspended solids concentration. Therefore, this model is selected as the optimal model for tidal suspended solids concentration inversion.

Validation of Turbidity Inversion Model

Accuracy validation was conducted for six turbidity inversion models based on SVR, RF, XGBoost, BO-SVR, BO-RF, and BO-XGBoost (Table 4).

Comparing the evaluation criteria of six turbidity inversion models, the model based on BO-XGBoost outperforms other models in all criteria. It achieved an R^2 value of 0.93, which is optimal among all models, and both RMSE and MAE achieved the minimum. Furthermore, by applying Bayesian Optimization, improvements were made to the SVR, RF, and XGBoost inversion models, resulting in a 10.8%, 5.9%, and 7.1% increase in R^2, respectively, demonstrating the effectiveness of Bayesian Optimization in enhancing the accuracy of inversion models. In summary, the BO-XGBoost model exhibits the highest accuracy and minimal errors in turbidity inversion; therefore, it is the optimal choice for tidal bore turbidity inversion.

Table 2. Pearson correlation coefficients between spectral characteristic parameters that meet the inversion requirements and water quality parameters.

Band and band combination	Suspension concentration		Turbidity	
	r	p	r	p
R5	0.613	0.000**	0.734	0.000**
R1-R4	-0.751	0.000**	-0.899	0.000**
R1-R5	-0.800	0.000**	-0.915	0.000**
R2-R3	-0.743	0.000**	-0.878	0.000**
R2-R4	-0.741	0.000**	-0.852	0.000**
R2-R5	-0.696	0.000**	-0.776	0.000**
R3-R4	-0.667	0.000**	-0.742	0.000**
R1/R3	-0.641	0.000**	-0.773	0.000**
R1/R4	-0.674	0.000**	-0.789	0.000**
R1/R5	-0.719	0.000**	-0.828	0.000**
R1/R6	-0.692	0.000**	-0.793	0.000**
R2/R3	-0.709	0.000**	-0.830	0.000**
R2/R4	-0.704	0.000**	-0.816	0.000**
R2/R5	-0.739	0.000**	-0.847	0.000**
R2/R6	-0.708	0.000**	-0.808	0.000**
R3/R4	-0.763	0.000**	-0.873	0.000**
R3/R5	-0.802	0.000**	-0.904	0.000**
R3/R6	-0.747	0.000**	-0.837	0.000**
R4/R5	-0.844	0.000**	-0.929	0.000**
R4/R6	-0.726	0.000**	-0.792	0.000**
(R1-R3)/(R1+R3)	-0.672	0.000**	-0.817	0.000**
(R1-R4)/(R1+R4)	-0.744	0.000**	-0.874	0.000**
(R1-R5)/(R1+R5)	-0.811	0.000**	-0.928	0.000**
(R1-R6)/(R1+R6)	-0.746	0.000	-0.844	0.000**
(R2-R3)/(R2+R3)	-0.741	0.000**	-0.869	0.000**
(R2-R4)/(R2+R4)	-0.778	0.000**	-0.898	0.000**
(R2-R5)/(R2+R5)	-0.833	0.000**	-0.940	0.000**
(R2-R6)/(R2+R6)	-0.756	0.000**	-0.843	0.000**
(R3-R4)/(R3+R4)	-0.795	0.000**	-0.904	0.000**
(R3-R5)/(R3+R5)	-0.851	0.000**	-0.945	0.000**
(R3-R6)/(R3+R6)	-0.709	0.000**	-0.776	0.000**
(R4-R5)/(R4+R5)	-0.866	0.000**	-0.943	0.000**

Inversion Results of Multispectral Images

Utilizing multispectral imagery, this study applied a Bayesian-optimized XGBoost (BO-XGBoost) model to invert suspended sediment concentration (SSC) in tidal bore environments at Qibao and Yanguan stations along the Qiantang River.

Table 3. Accuracy verification of suspended solids concentration inversion models.

Water quality parameters	Model	Evaluation indicators		
		R^2	*RMSE*/mg·L^{-1}	*MAE*/mg·L^{-1}
Suspended solids concentration	SVR	0.69	450.54	420.45
	RF	0.82	412.52	401.35
	XGBoost	0.85	380.55	350.54
	BO-SVR	0.78	401.58	370.65
	BO-RF	0.86	350.41	336.44
	BO-XGBoost	0.89	310.54	280.24

Inversion Results in Suspended Solids Concentration

Fig. 4 details the inversion results of suspended sediment concentration (SSC) at Qibao Station on the Qiantang River. As shown in Fig. 4, the retrieved and measured SSC values at five sampling points during the monitoring process exhibit strong agreement, with a coefficient of determination (R^2) of 0.91, root mean square error (RMSE) of 4.61 mg/L, and mean absolute error (MAE) of 4.24 mg/L, indicating high model accuracy.

Similarly, the SSC inversion results for Yanguan Station are presented in Fig. 4. The comparison between retrieved and measured SSC values demonstrates robust consistency, achieving an R^2 of 0.92, RMSE of 312.7 mg/L, and MAE of 230.5 mg/L. Notably, while both stations show strong model performance, the elevated RMSE and MAE at Yanguan Station likely reflect the intensified hydrodynamic turbulence characteristic of this tidal bore-dominated reach.

Turbidity Inversion Results

Fig. 5 details the turbidity inversion results for Qibao Station on the Qiantang River. As depicted in Fig. 5, the retrieved and measured turbidity values across five sampling points during the monitoring process exhibit strong agreement, with a coefficient of determination (R^2) of 0.95, root mean square error (RMSE) of 3.24 NTU, and mean absolute error (MAE) of 2.92 NTU, underscoring the model's precision in low-turbulence environments.

Fig. 5 details the turbidity inversion results for Yanguan Station. The comparison between retrieved and measured values demonstrates robust consistency, yielding an R^2 of 0.93, RMSE of 24.9 NTU, and MAE of 22.8 NTU. The relatively higher errors at Yanguan Station align with its exposure to intensified tidal bore dynamics, which amplify suspended sediment variability and optical complexity.

Discussion

Machine Learning Model Performance

A total of 90 preprocessed datasets were partitioned into a sample set, with approximately three-sevenths allocated for training and the remainder reserved for testing. During model development, the optimal feature subsets derived from spectral parameter optimization were employed as independent variables, while in-situ water quality measurements served as dependent variables, enabling the construction of tidal bore water quality inversion models using Support Vector Regression (SVR), Random Forest (RF), and eXtreme Gradient Boosting (XGBoost). Additionally, Bayesian Optimization was applied to refine hyperparameters for each algorithm, yielding enhanced models: Bayesian-Optimized SVR (BO-SVR), Bayesian-Optimized RF (BO-RF), and Bayesian-Optimized XGBoost (BO-

Table 4. Accuracy validation of turbidity inversion models.

Water quality parameters	Model	Evaluation indicators		
		R^2	*RMSE*/NTU	*MAE*/NTU
Turbidity	SVR	0.65	65.36	61.06
	RF	0.85	58.93	56.37
	XGBoost	0.87	53.36	49.05
	BO-SVR	0.72	57.38	54.98
	BO-RF	0.90	40.75	38.86
	BO-XGBoost	0.93	33.36	30.43

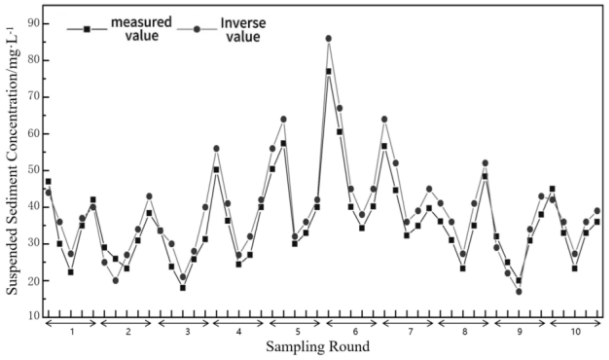

(a) Temporal Variation of Suspended Sediment Concentration Inversion Results at Qibao Station

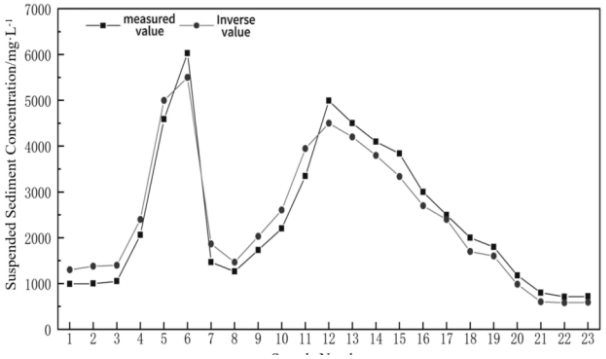

(b) Temporal Variation of Suspended Sediment Concentration (SSC) Inversion Results at Yanguan Station

Fig. 4. Temporal Variation of SSC Inversion Results: (a) Qibao Station; (b) Yanguan Station.

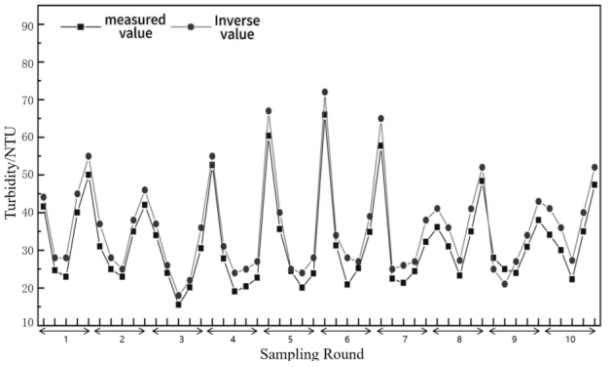

(a) Temporal Variation of Turbidity Inversion Results at Qibao Station

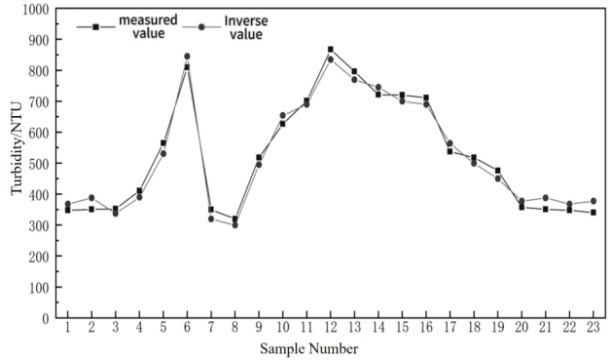

(b) Temporal Variation of Turbidity Inversion Results at Yanguan Station

Fig. 5. Temporal Variation of Turbidity Inversion Results: (a) Qibao Station; (b) Yanguan Station.

XGBoost). This framework developed six distinct inversion models—SVR, RF, XGBoost, BO-SVR, BO-RF, and BO-XGBoost— for estimating both suspended sediment concentration (SSC) and turbidity in tidal bore environments.

In order to visually compare the inversion results of each model, the study conducted a linear fitting analysis between the observed values and the model-predicted values for suspended solids concentration (Fig. 6). From the figure, it can be observed that the slope of the fitted line for the model based on BO-XGBoost reaches 0.87, and the water quality parameter data points are the closest approach to the 1:1 trend line. This indicates the model's performance is optimal, and its estimation level is robust. Therefore, the suspended solids inversion model based on BO-XGBoost is suitable for estimating the concentration of suspended solids in the Qiantang River tidal bore area.

To visually compare the inversion performance of each model, the study conducted linear fitting of the turbidity ground truth values and the model inversion values for each model (Fig. 7). The graph shows that the turbidity inversion model based on BO-XGBoost has a slope of 0.91, and the water quality parameter data points were the closest approach to the 1:1 trend line. This indicates the model's performance is optimal, and its estimation level is robust. Therefore, the turbidity inversion model based on BO-XGBoost is suitable for estimating the turbidity concentration in the Qiantang River tidal bore area.

In this study, we selected representative traditional regression algorithms from the machine learning domain – Support Vector Regression (SVR), Random Forest (RF), and eXtreme Gradient Boosting (XGBoost) – to develop water quality inversion models for the Qiantang River tidal bore. Bayesian Optimization was further applied to refine hyperparameters for these models, and their performance was evaluated using metrics including the coefficient of determination (R^2), mean absolute error (MAE), and root mean square error (RMSE). Comparative analysis revealed that the BO-XGBoost model outperformed other algorithms in both SSC and turbidity inversion, thereby establishing it as the optimal model for tidal bore water quality retrieval.

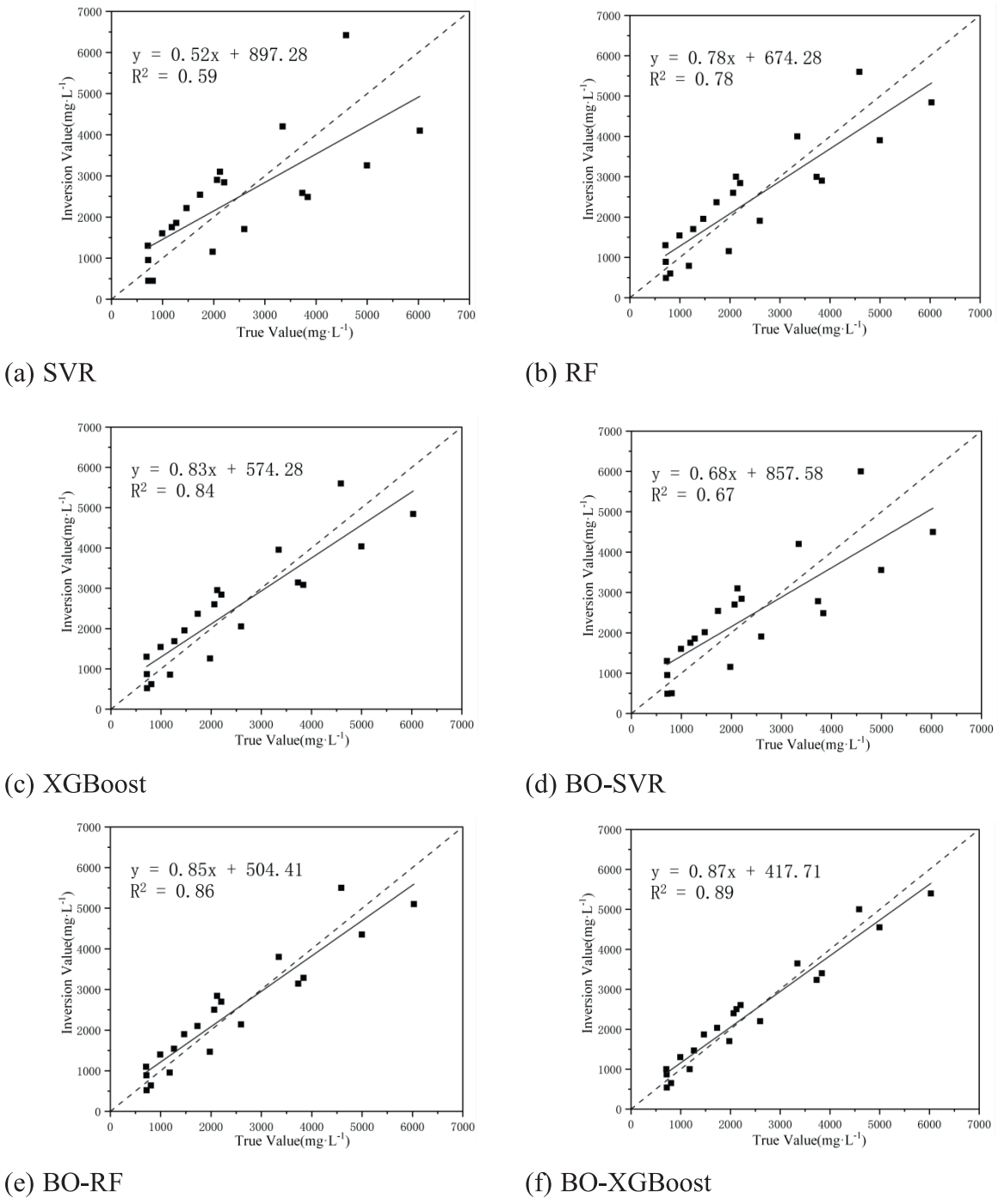

Fig. 6. Scatter plot of observed and predicted suspended solids concentrations.

Discussion of Water Quality Inversion Results

1. Suspended Sediment Concentration Inversion in the Qiantang River

Inversion models for tidal bore suspended solids concentration were constructed using BO-XGBoost based on multispectral imagery data. The suspended solids concentration at Qiantang River Qibao Station and Yanguan Station was inverted.

According to the inversion data from each sampling point, it was found that the suspended solids concentrations at sampling points A and E of the Qibao Station were relatively high, reaching up to about 80 mg/L, while the concentrations at sampling points B, C, and D were relatively lower, around 18 mg/L. This phenomenon may be related to factors such as estuarine topography and hydrodynamics. Influenced by the topography and hydrodynamic characteristics, the water depth in the center of the river is greater than that on both banks, and the flow velocity is relatively faster, which is conducive to the transport and dilution of suspended solids, resulting in relatively lower concentrations in these areas. Conversely, due to the shallower water depth and slower flow velocity in shallow water areas near the

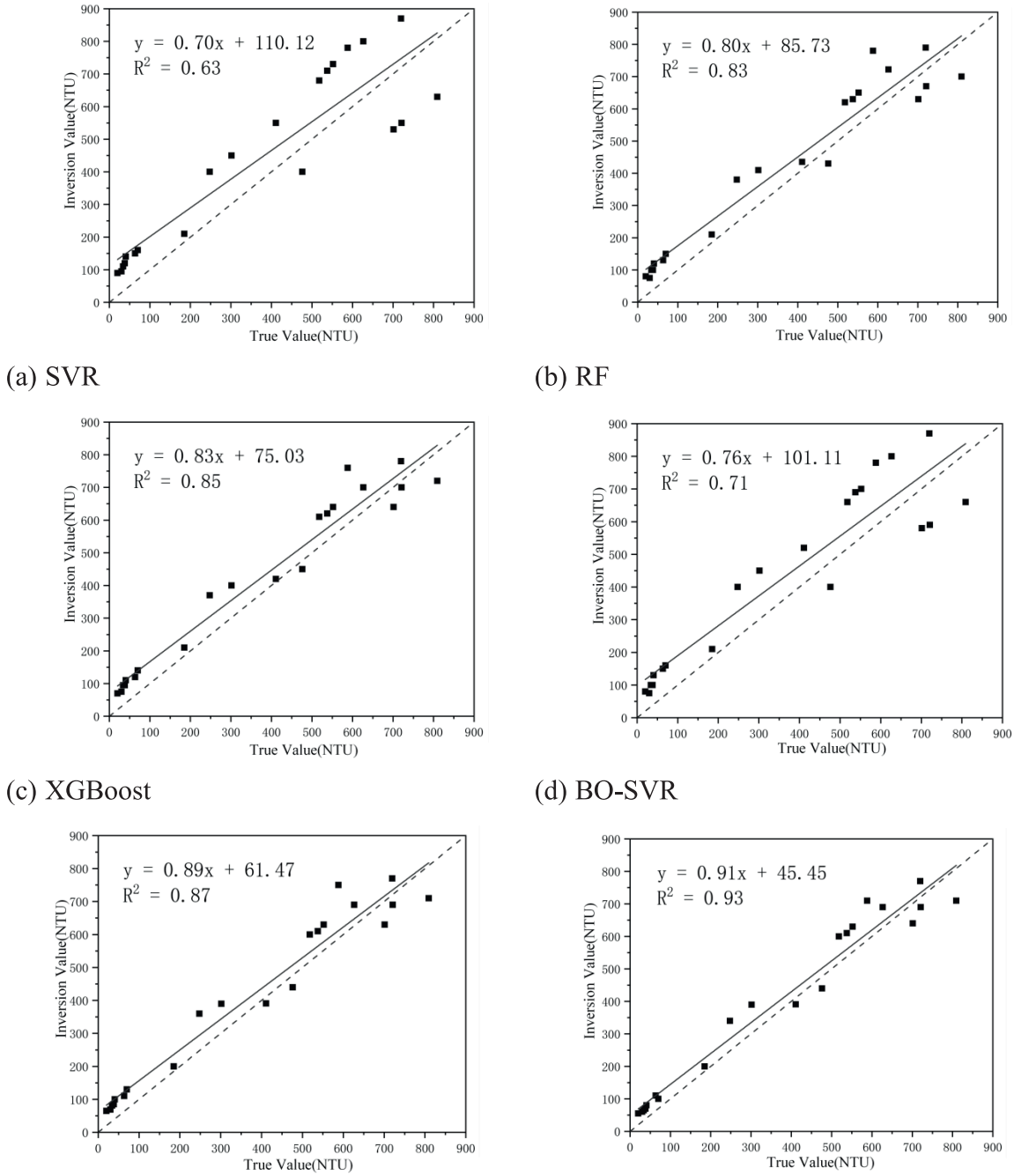

Fig. 7. Scatter plot of turbidity ground truth values and inversion values.

shore, suspended solids are more likely to deposit here, leading to relatively higher concentrations of suspended solids.

Fig. 8 represents the results of 8 out of 23 samples taken at the Yanguan Station, providing an overview of the suspended solids concentration variations during the tidal bore. Fig. 8 shows that the distribution of suspended solids concentration at the Yanguan Station was relatively stable during the first three sampling events. However, during the fourth sampling event, especially near the two piers, a significant change in suspended solids concentration distribution occurred, reaching a maximum of approximately 6000 mg/L. This change is likely due to the abrupt flow velocity and direction alteration when the tidal surge arrives, particularly the drastic changes in the near-bottom flow field. The strong turning current, coupled with complex turbulence and vortex structures, scours the bed and causes a large number of fine sediment particles to be suspended, leading to a sharp increase in suspended solids concentration in the water. This change is particularly evident near the piers, as they hinder the flow, intensifying the effects of turbulence and vortices. The flow velocity slows as the flood tide weakens, and

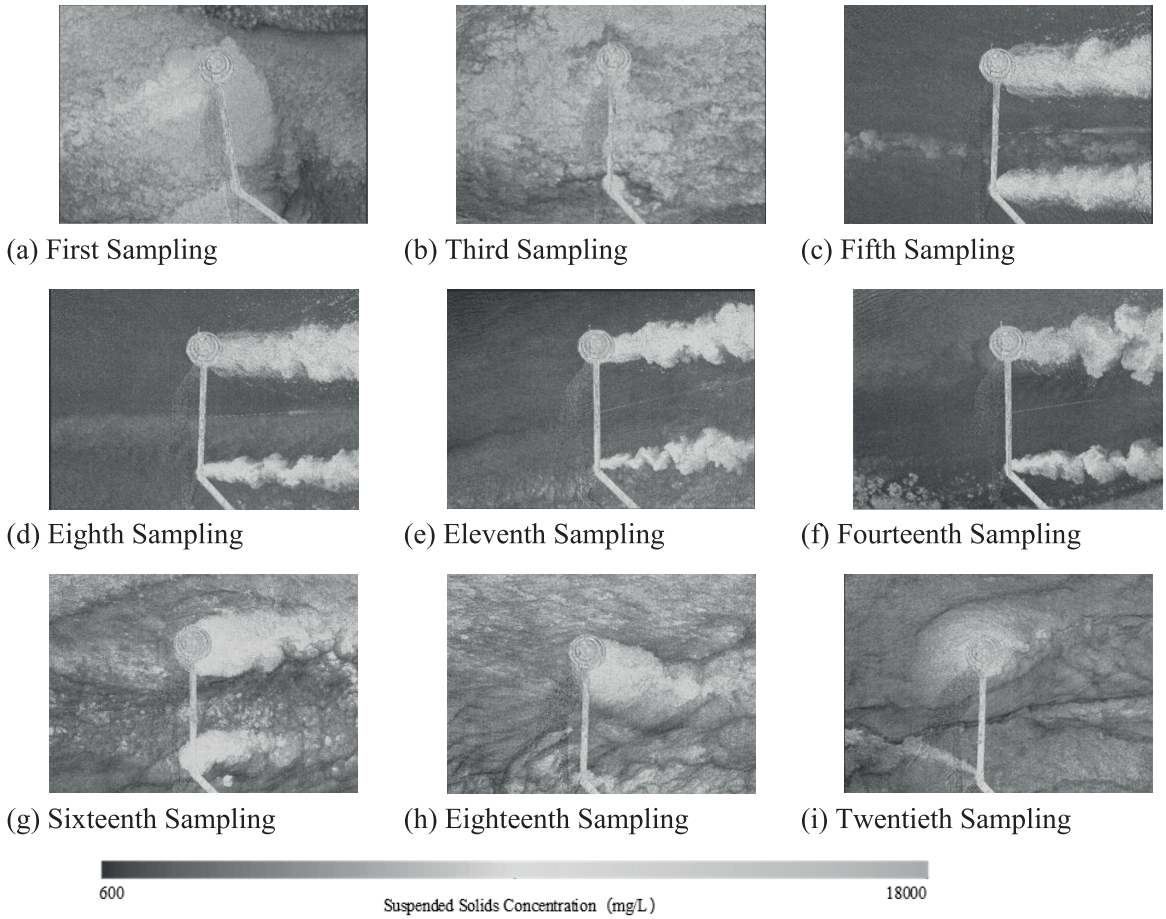

Fig. 8. Inversion of Suspended Particulate Matter Concentration at Yanguan Station.

the suspended solids concentration gradually decreases, eventually reaching a relatively stable state. At this point, the suspended solids concentration at the sampling point is approximately 3900 mg/L, as observed in the inversion graph of the twentieth sampling event.

In summary, the research results indicate that the suspended solids concentration exhibits significant spatial variations due to the combined effects of environmental factors such as water depth, typically manifested as a trend of lower concentration in the center and higher concentration on both banks. Additionally, the influence of tidal surges on the suspended solids concentration is also significant. During the flood tide period, as the tidal surge intensity increases, there is a notable increase in suspended solids concentration, particularly near the piers where the changes are more pronounced.

2. Turbidity Inversion in the Qiantang River

Inversion models for tidal bore turbidity were constructed using BO-XGBoost based on multispectral imagery data. The turbidity at Qiantang River Qibao Station and Yanguan Station was inverted.

Based on the inversion data from each sampling point, the turbidity at sampling points A and E in Qibao Station is relatively high, reaching a maximum of approximately 65 NTU, while the turbidity at sampling points B, C, and D is relatively lower, around 15 NTU. This phenomenon may be influenced by topography and hydrodynamic characteristics. The water depth in the center of the river is typically greater than that of the two banks, and areas with greater water depth usually have faster water flow velocities, which facilitates the transport and dilution of suspended particles. As a result, the turbidity is relatively lower in these areas. Conversely, in the shallow water areas near the shoreline, where water flow velocities are slower, suspended particles are more prone to deposit in this region, resulting in higher turbidity.

Fig. 9 shows the results of 9 out of 23 samplings at Yanguan Station, revealing the turbidity distribution during the tidal surging period. In the first three samplings, the turbidity distribution remained relatively stable. However, during the fourth sampling, particularly near the two piers, there was a sudden and significant change in turbidity distribution, reaching a maximum of approximately 820 NTU. This change is likely due to the rapid alteration in water velocity and direction with the arrival of the tidal surge, especially in the near-bottom flow field, where intense changes occur. The strong turning water flow, combined with complex turbulence and vortex structures, scours the bottom bed, causing a large amount of fine sediment to rise and

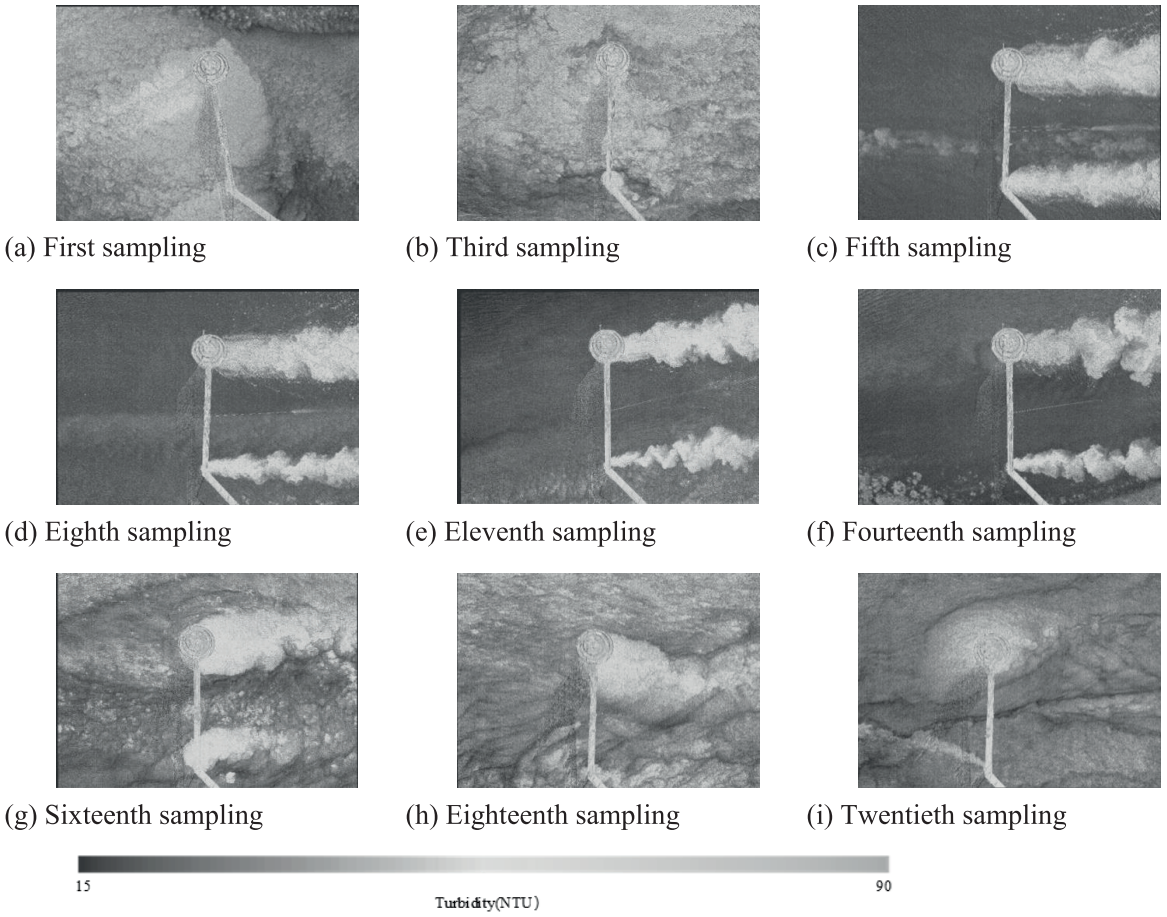

Fig. 9. Turbidity inversion plot of the Yanguan Station.

sharply increase the turbidity in the water. This change is particularly evident near the piers, as they obstruct the flow, intensifying the effects of turbulence and eddies. As the flood tide weakens and the flow velocity slows down, the turbidity gradually decreases and tends to stabilize. At this point, the turbidity at the sampling point is approximately 312 NTU, as observed in the inversion map of the twentieth sampling.

The above analysis results are consistent with the measured data, validating the feasibility of multispectral imagery and machine learning inversion models in tidal bore water quality monitoring.

Application and Implications of Water Quality Inversion

This study developed inversion models for suspended sediment concentration (SSC) and turbidity in the Qiantang River tidal bore by integrating drone-based multispectral remote sensing with Bayesian-optimized machine learning algorithms. The results demonstrated significant negative correlations between normalized spectral indices (e.g., (R4-R5)/(R4+R5)) and both SSC and turbidity, revealing the sensitivity of shortwave bands (R4, R5) to fine-grained suspended particles. The BO-XGBoost model substantially outperformed conventional models, achieving determination coefficients (R^2) of 0.89 for SSC and 0.93 for turbidity. Spatial analysis identified a distinct "low-center, high-bank" distribution pattern, with SSC surges near bridge piers during flood tides (exceeding 6,000 mg/L) due to turbulent scouring. The strong correlation ($R^2 > 0.90$) between SSC and turbidity validated turbidity as a reliable proxy for SSC in dynamic tidal environments. Both parameters exhibited synchronous spatiotemporal trends, escalating sharply with intensified tidal bore dynamics, particularly near engineered structures like bridge piers.

Compared to traditional satellite remote sensing for water quality inversion, the drone-based multispectral imagery employed in this study significantly enhanced spatial resolution, enabling precise detection of minor water quality variations under transient tidal bore disturbances. While retaining a consistent inversion framework, Bayesian Optimization effectively mitigates model overfitting. Algorithmically, whereas prior studies predominantly focused on Support Vector Regression (SVR) and Random Forest (RF), this work demonstrates XGBoost's superiority in modeling nonlinear water quality parameters. When integrated with Bayesian hyperparameter tuning, the approach achieved a 37% improvement in optimization efficiency over conventional grid search methods. High-frequency

imagery revealed the acute impacts of instantaneous tidal bore dynamics on water quality, particularly in areas with dense hydraulic infrastructure. This addresses a critical gap in short-term hydrodynamic monitoring theory.

The high correlation of spectral feature parameters originates from the absorption-scattering effects of suspended particles on specific wavelength bands. For instance, shortwave bands (R4, R5) exhibit enhanced sensitivity to fine-grained sediments, a finding that provides a physical basis for optimizing multispectral band combinations in remote sensing applications. The superior accuracy of the BO-XGBoost model underscores Bayesian Optimization's capability to probabilistically explore global parameter spaces, effectively circumventing local optima traps inherent in traditional hyperparameter tuning methods. This establishes an efficient algorithmic framework for water quality inversion in complex hydrodynamic environments. Furthermore, abrupt SSC surges near bridge piers reveal the hydrodynamic perturbations induced by hydraulic infrastructure, highlighting the necessity to prioritize assessments of engineering layouts for their potential risks – such as bed erosion and ecosystem disruption – in estuarine management. These insights offer a scientific foundation for water quality governance in tide-sensitive zones.

The strengths of this study are threefold. (1) Integration of drone platforms with synchronized in-situ measurements enabled high spatiotemporal-resolution dynamic monitoring of tidal bore water quality; (2) Incorporation of Bayesian Optimization into estuarine water quality inversion significantly enhanced model accuracy and generalizability; and (3) The inversion results directly support the development of an early-warning system for water quality along the Qiantang River, demonstrating substantial practical engineering value. However, several limitations warrant consideration. (1) Data collection was limited to two tidal bore events, lacking coverage of seasonal or extreme tidal conditions that drive water quality variability; (2) The model's optimization efficacy, validated in the Qiantang River's specific reaches, requires further validation across diverse geomorphic estuaries to confirm its universality; and (3) The exclusion of environmental covariates (e.g., wind speed, water temperature) may compromise model robustness under complex meteorological conditions.

This study demonstrates that the integration of drone-based multispectral remote sensing with Bayesian-optimized machine learning models can efficiently invert spatiotemporal dynamics of water quality parameters in tidal estuaries, offering a high-accuracy, low-cost technical pathway for tidal bore monitoring. Future efforts should prioritize (1) Extending data collection periods to encompass multi-seasonal and variable tidal intensity scenarios, enhancing model adaptability; (2) Integrating hydrological models with meteorological satellite data to establish a multi-source-driven inversion framework; (3) Developing edge computing-enabled drone systems for real-time monitoring and rapid anomaly alerting. With these advancements, the proposed methodology holds promise as a robust tool for tidal estuary water quality management, providing critical technological support for estuarine ecological conservation and sustainable development.

Discussion

This study focused on the Qiantang River Qibao and Yanguan stations, using water quality data collected during the tidal bore on November 16th and 28th, 2023, and the simultaneous acquisition of multispectral remote sensing images. A machine learning-based model for water quality inversion in the Qiantang River tidal bore was constructed and applied. The main conclusions are as follows:

This study used the Pearson correlation coefficient to evaluate the correlation between spectral feature parameters and various water quality parameters. The results showed that the correlation between total nitrogen and total phosphorus and spectral feature parameters was generally low and did not meet the requirements for inversion. The correlation between suspended solids concentration, turbidity, and single-band spectral feature parameters was generally low, but their correlation with spectral feature parameters constructed using the ratio index and normalized index was high. Among all spectral feature parameters, (R4-R5)/(R4+R5) showed the most significant correlation with suspended solids concentration and turbidity, with the highest absolute correlation coefficient reaching 0.866 for suspended solids concentration and 0.943 for turbidity, indicating a strong correlation.

This study constructed Support Vector Machine (SVM), Random Forest (RF), and Extreme Gradient Boosting (XGBoost) models based on the optimal feature subset and measured water quality parameters. The Bayesian Optimization algorithm optimized these three machine learning models, resulting in six tidal surge water quality inversion models. By comprehensively comparing each model's evaluation metric and fitting accuracy, the inversion models for suspended solids concentration and turbidity based on the BO-XGBoost model showed the highest monitoring accuracy, with a coefficient of determination reaching 0.89 and 0.93, respectively. The models exhibited stable estimation performance and can be considered optimal inversion solutions for water quality in the Qiantang River tidal surge.

Based on the multispectral image data, the suspended solids concentration and turbidity inversion models constructed using BO-XGBoost were applied to invert the suspended solids concentration and turbidity at the Qiantang River Qibao and Yanguan stations. The laws of spatiotemporal variation and influencing mechanisms were analyzed. The analysis results were consistent

with the measured data, validating the feasibility of multispectral imagery and machine learning inversion models in tidal surge water quality monitoring. Further analysis indicated that the suspended solids concentration and turbidity tended to increase in the center and decrease at the two banks. Additionally, the influence of tidal surges on suspended solids concentration and turbidity was significant. During the rising tide, the tidal surge dynamics strengthened. The suspended solids concentration significantly increased, especially near the bridge piers, where the variations were more pronounced. Furthermore, the analysis revealed that the spatiotemporal variation trends of turbidity and suspended solids concentration were generally consistent.

Acknowledgments

This research was supported by the Joint Funds of the Zhejiang Provincial Natural Science Foundation of China under Grant No. LZJWY24E090002. This research was supported by the Funds of Scientific Research Institutes for the Provincial Institute of Zhejiang under Grant No. ZIHEYS23002.

Conflict of Interest

The authors declare no conflict of interest.

References

1. HUANG J., PAN C., KUANG C., ZENG J., CHEN G. Experimental hydrodynamic study of the Qiantang River tidal bore. Journal of Hydrodynamics, **25**, 481, **2013**.
2. FAN D., CAI G., SHANG S., WU Y., ZHANG Y., GAO L. Sedimentation processes and sedimentary characteristics of tidal bores along the north bank of the Qiantang Estuary. Chinese Science Bulletin, **57**, 1578, **2012**.
3. XIE D., PAN C., WU X., GAO S., WANG Z.B. The variations of sediment transport patterns in the outer Changjiang Estuary and Hangzhou Bay over the last 30 years. Journal of Geophysical Research, **122**, 2999, **2017**.
4. SHI Y.-B., CHENG W.-L. Law of Salt Tide Intrusion of the Qiantang Estuary and Its Numerical Simulation. Springer Singapore, Singapore, **2020**.
5. LI R., GAO L., PAN C., PANG Y. Detecting the mechanisms of longitudinal salt transport during spring tides in Qiantang Estuary. Journal of Integrative Environmental Sciences, **16** (1), 123, **2019**.
6. XIE D., PAN C., GAO S., WANG Z.B. Morphodynamics of the Qiantang Estuary, China: Controls of river flood events and tidal bores. Marine Geology, **406**, 27, **2018**.
7. XIE D., HUANG J., BO J., LI R., TANG Z., LU H. A preliminary study on seasonal variations of sediment concentrations in the inner Qiantang Estuary. IOP Conference Series: Earth and Environmental Science, **569**, **2020**.
8. WAI O.W.H., WANG C.H., LI Y.S., LI X.D. The formation mechanisms of turbidity maximum in the Pearl River estuary, China. Marine Pollution Bulletin, **48** (5), 441, **2004**.
9. CHANSON H. Current knowledge in tidal bores and their environmental, ecological and cultural impacts. Environmental Fluid Mechanics, **11** (1), 77, **2011**.
10. LI L., JIANG P., XU H., LIN G., GUO D., WU H. Water quality prediction based on recurrent neural network and improved evidence theory: a case study of Qiantang River, China. Environmental Science and Pollution Research, **26** (19), 19879, **2019**.
11. HUANG F., WANG X., LOU L., ZHOU Z., WU J. Spatial variation and source apportionment of water pollution in Qiantang River (China) using statistical techniques. Water Research, **44** (5), 1562, **2010**.
12. YI-NAN L., ZHI-LIN S., YUN G. Influence of Topographical Descending on Saltwater Intrusion in Qiantang River. Journal of Yangtze River Scientific Research Institute, **2015**.
13. GLASGOW H.B., BURKHOLDER J.M., REED R.E., LEWITUS A.J., KLEINMAN J.E. Real-time remote monitoring of water quality: a review of current applications, and advancements in sensor, telemetry, and computing technologies. Journal of Experimental Marine Biology and Ecology, **300** (1), 409, **2004**.
14. JIAO J.-G., HUANG S.-J., ZHENG R. Influence of Tide and Runoff on Saltwater Intrusion in the Qiantang River Estuary, China. IOP Conference Series: Earth and Environmental Science, **691**, **2021**.
15. PALMER S.C.J., KUTSER T., HUNTER P.D. Remote sensing of inland waters: Challenges, progress and future directions. Remote Sensing of Environment, **157**, 1, **2015**.
16. AMADOR-CASTRO F., GONZáLEZ-LóPEZ M.E., LOPEZ-GONZALEZ G., GARCIA-GONZALEZ A., DíAZ-TORRES O., CARBAJAL-ESPINOSA O., GRADILLA-HERNáNDEZ M.S. Internet of Things and citizen science as alternative water quality monitoring approaches and the importance of effective water quality communication. Journal of Environmental Management, **352**, 119959, **2024**.
17. WORACHAIRUNGREUNG M., KULPANICH N., THANAKUNWUTTHIROT K., HEMWAN P. Monitoring Agricultural Land Loss by Analyzing Changes in Land Use and Land Cover. Emerging Science Journal, **2024**.
18. GUIMARãES T.T., VERONEZ M.R., KOSTE E.C., SOUZA E.M., BRUM D., GONZAGA L., MAUAD F.F. Evaluation of Regression Analysis and Neural Networks to Predict Total Suspended Solids in Water Bodies from Unmanned Aerial Vehicle Images. Sustainability, **11** (9), 2580, **2019**.
19. YAN Y., WANG Y., YU C., ZHANG Z. Multispectral Remote Sensing for Estimating Water Quality Parameters: A Comparative Study of Inversion Methods Using Unmanned Aerial Vehicles (UAVs). Sustainability, **15** (13), 10298, **2023**.
20. ADJOVU G.E., STEPHEN H., JAMES D., AHMAD S. Overview of the Application of Remote Sensing in Effective Monitoring of Water Quality Parameters. Remote Sensing, **15** (7), 1938, **2023**.
21. MATSUI K., SHIRAI H., KAGEYAMA Y., YOKOYAMA H. Improving the resolution of UAV-based remote sensing data of water quality of Lake Hachiroko, Japan by neural networks. Ecological Informatics, **62**, 101276, **2021**.
22. ZANG W.Q., LIN J.Y., WANG Y.C., TAO H. Investigating small-scale water pollution with UAV Remote Sensing Technology, **2012**.

23. MCELIECE R., HINZ S., GUARINI J.M., COSTON-GUARINI J. Evaluation of Nearshore and Offshore Water Quality Assessment Using UAV Multispectral Imagery. Remote. Sens, **12**, 2258, **2020**.
24. HOOGENBOOM H.J., DEKKER A.G., ALTHUIS I.A. Simulation of AVIRIS Sensitivity for Detecting Chlorophyll over Coastal and Inland Waters. Remote Sensing of Environment, **65**, 333, **1998**.
25. BREZONIK P.L., MENKEN K.D., BAUER M.E. Landsat-based Remote Sensing of Lake Water Quality Characteristics, Including Chlorophyll and Colored Dissolved Organic Matter (CDOM). Lake and Reservoir Management, **21**, 373 **2005**.
26. MA Z., WANG L., LI X., QU X., YIN J., ZHAO X., LIU Y. The oasis regional small and medium lake water transparency monitoring research and impact factor analysis based on field data combined with high resolution GF-1 satellite data. Journal of Freshwater Ecology, **36**, 77 **2021**.
27. TIAN S., GUO H., XU W., ZHU X., WANG B., ZENG Q., MAI Y., HUANG J.J. Remote sensing retrieval of inland water quality parameters using Sentinel-2 and multiple machine learning algorithms. Environmental Science and Pollution Research, **30** (7), 18617, **2023**.
28. LEI F., YU Y., ZHANG D., FENG L., GUO J., ZHANG Y., FANG F. Water remote sensing eutrophication inversion algorithm based on multilayer convolutional neural network. Journal of Intelligent & Fuzzy Systems, **39** (1), 5319, **2020**.
29. ZHU M., WANG J., YANG X., ZHANG Y., ZHANG L., REN H., WU B., YE L. A review of the application of machine learning in water quality evaluation. Eco-Environment & Health, **1** (2), 107, **2022**.
30. PETERSON K.T., SAGAN V., SLOAN J.J. Deep learning-based water quality estimation and anomaly detection using Landsat-8/Sentinel-2 virtual constellation and cloud computing. GIScience & Remote Sensing, **57**, 510 **2020**.
31. PARK Y., CHO K.H., PARK J., CHA S.M., KIM J.H. Development of early-warning protocol for predicting chlorophyll-a concentration using machine learning models in freshwater and estuarine reservoirs, Korea. Science of The Total Environment, **502**, 31, **2015**.
32. KRISHNARAJ A., HONNASIDDAIAH R. Remote sensing and machine learning based framework for the assessment of spatio-temporal water quality in the Middle Ganga Basin. Environmental Science and Pollution Research, **29** (43), 64939, **2022**.
33. ISMAIL R., RAWASHDEH A., AL-MATTARNEH H., HATAMLEH R., TELFAH D.A.B., JARADAT A. Artificial Intelligence for Application in Water Engineering: The Use of ANN to Determine Water Quality Index in Rivers. Civil Engineering Journal, **10**, 2261, **2024**.
34. RATTANARAT J., JAROENSUTASINEE K., JAROENSUTASINEE M., SPARROW E. Government Policy Influence on Land Use and Land Cover Changes: A 30-Year Analysis. Emerging Science Journal, **8**, 1783, **2024**.
35. LE K.D., NGUYEN G.T. Applying Harmony Degree Equation and TOPSIS Combined with Entropy Weights in Surface Water Classification. Civil Engineering Journal, **2024**.
36. SHARMA J., KANAKIYA R., SINGH S. Characterisation Study and Correlation Analysis For Water Quality of Dal Lake, India. International Journal of Lakes and Rivers. ISSN 0973-4570, **8**, 25, **2015**.
37. CHEN Q., MENG Z., LIU X., JIN Q., SU R. Decision Variants for the Automatic Determination of Optimal Feature Subset in RF-RFE. Genes, **9**, **2018**.
38. TIAN Y., ZHANG J., YAO X., CAO W., ZHU Y. Laboratory assessment of three quantitative methods for estimating the organic matter content of soils in China based on visible/near-infrared reflectance spectra. Geoderma, **202-203**, 161, **2013**.
39. DRUCKER H., BURGES C.J.C., KAUFMAN L., SMOLA A., VAPNIK V.N. Support Vector Regression Machines, **1996**.
40. BREIMAN L. Random Forests. Machine Learning, **45** (1), 5, **2001**.
41. CHEN T., GUESTRIN C. XGBoost: A Scalable Tree Boosting System. Proceedings of the 22nd ACM SIGKDD International Conference on Knowledge Discovery and Data Mining, **2016**.
42. FRAZIER P.I. Bayesian Optimization. Recent Advances in Optimization and Modeling of Contemporary Problems, **2018**.
43. SCHNEIDER P.I., SANTIAGO X.G., ROCKSTUHL C., BURGER S. Global optimization of complex optical structures using Bayesian optimization based on Gaussian processes, **2017**.
44. CANDELIERI A., PEREGO R., ARCHETTI F. Bayesian optimization of pump operations in water distribution systems. Journal of Global Optimization, **71**, 213, **2018**.